Electric double layer in ionic liquids: A result of interplay between coupling effects and phase demixing

YeongKyu Lee*
Korea Institute for Advanced Study, Seoul 02455, Korea

JunBeom Cho,* Yongkyu Lee, and Won Bo Lee†
School of Chemical and Biological Engineering, Seoul National University, Seoul 08826, Republic of Korea

YongSeok Jho‡
Department of Physics and Research Institute of Molecular Alchemy, Gyeongsang National University, 52828 Jinjudae-ro 501, Republic of Korea

(Received 2 January 2024; accepted 17 June 2024; published 8 July 2024)

Ionic liquids (ILs) are appealing electrolytes for their favorable physicochemical properties. However, despite their longstanding use, understanding the capacitive behavior of ILs remains challenging. This is largely due to the formation of a nonconventional electric double layer (EDL) at the electrode-electrolyte interface. This study shows that the short-range Yukawa interactions, representing the large anisotropically charged ILs, demix IL to create a spontaneous surface charge separation, which is reinforced by the strongly coupled charge interaction. The properties of the condensed layer, the onset of charge separation, and the rise of overscreening and crowding critically depend on the asymmetry of Yukawa interactions.

DOI: 10.1103/PhysRevResearch.6.033026

I. INTRODUCTION

Room-temperature ionic liquids (RTILs) are combinations of large organic cations and organic, inorganic anions with delocalized charges. Unlike conventional inorganic salts, these structural characteristics prevent them from forming crystalline structures at room temperature [1–3]. As an electrolyte solvent at ambient conditions, RTILs offer several advantages for energy storage applications, such as low volatility, good solvent properties, high thermal stability, and environmental sustainability [4–9], which are especially fit for future energy storage devices, supercapacitors, or ultracapacitors. Notably, some essential features for high-technology devices (e.g., wireless devices and electric cars), such as higher-rate energy harvesting and long-lasting supercapacitance, are related to the electric double layer (EDL) structures in RTILs [10–14]. While conventional point-charge models predict the development of a condensation layer at very large surface charge densities, IL exhibits EDL at very low surface charge densities and even overscreening and crowding, which are very difficult to achieve without the presence of the multivalent counterions within the point-charge models. The key differences are from the large shape of IL molecules and their delocalized charges. Understanding how to embody these properties in the microscopic mechanism is challenging and crucial in utilizing ILs for energy device applications [15–18].

Bazant, Storey, and Korneyshev (BSK) [19] are among the first to incorporate a short-range electrostatic correlation to the EDL. They showed that a phenomenological modification of the Poisson equation with an extra fourth-order potential gradient term, reflecting a short-range electrostatic correlation, explains the divergence of differential capacitance. They further asserted that crowding beats overscreening at higher external fields. Since the phenomenological description of the BSK model, efforts have been made to uncover the microscopic mechanism for unconventional EDL features. Démery *et al.* solved one-dimensional (1D) lattice Coulomb gas (1D LCG) under the constant-voltage ensemble. Their solvable one-dimensional model showed that the 1D LCG undergoes a first-order phase transition between dense and dilute phases by adjusting fugacity [20,21]. They claimed the transition is closely related to the discontinuous jump in differential capacitance and the transition between camel- and bell-shape capacitance. Limmer constructed a phenomenological model of dense ionic solutions near the charged planar wall. He found that charge-density ordering at the interface results in the divergence of the differential capacitance [22].

Other directions of the approaches use statistical field theory for charged many body. Earlier mobile point charges with fixed macroions were treated within the framework of the statistical field theory of ion systems [15,23–26]. Recently, Bossa *et al.* adopted the free-energy analysis approaches incorporating Yukawa potential to consider the symmetric steric term and successfully reproduced the fourth-order potential

*These authors contributed equally to this work.
†Contact author: wblee@snu.ac.kr
‡Contact author: ysjho@gnu.ac.kr

gradient in BSK equation [27,28]. They showed that the interplay between short-ranged Yukawa and long-ranged Coulomb interactions can lead to the instability of ILs near an electrode. This instability is characterized by a divergent differential capacitance, indicating a first-order transition [27].

This work uncovers the microscopic origin of the unconventional EDL formation and the consequent phase transition of RTIL capacitance employing a statistical field-theory framework. We derive free-energy functionals for asymmetric ionic liquids and extracted the modified Poisson equations via saddle-point approximation. Our results reveal that the phase transition is triggered by the interplay of the strong electrostatic coupling and the phase demixing due to the asymmetric short-range interaction. We validate our theoretical predictions by comparing them with molecular dynamics simulations. We further elucidate the influence of external electric fields on the phase behavior. This work potentially applies to the various systems related to the multipolar solvents electrostatics, and the spontaneous surface absorption of polyelectrolytes [29–34].

II. FIELD THEORETIC MODEL

We develop a lattice-based model for the electrode of surface charge density σ_e at $x = 0$. The number of the particle at r is $n_\pm(r)$ and $\sum_r n_\pm = N_\pm$. The local densities of each species are $\rho_\pm(r) = n_\pm(r)/v$, where v is the volume of each lattice. The local charge density is defined as $\rho_c(r) = \rho_+(r) - \rho_-(r)$.

Particles interact with each other through Coulombic and Yukawa interaction:

$$\begin{aligned}\beta u_{+,+} &= \frac{l_B}{r} + a\frac{e^{-\kappa r}}{r},\\ \beta u_{+,-} &= -\frac{l_B}{r} + c\frac{e^{-\kappa r}}{r},\\ \beta u_{-,-} &= \frac{l_B}{r} + b\frac{e^{-\kappa r}}{r},\end{aligned} \tag{1}$$

where l_B is the Bjerrum length, and a, b, and c are the Yukawa interaction parameters, and $\beta = \frac{1}{k_B T}$. Then, the total interaction potential energy is represented by

$$\begin{aligned}\beta\mathcal{U}_{\rm tot} = &\frac{1}{2}\int dr dr' \rho_c(r) v_c(r-r')\rho_c(r')\\ &+ \frac{1}{2}\int dr dr' \begin{pmatrix}\rho_+(r)\\ \rho_-(r)\end{pmatrix}^T A_h v_y(r-r') \begin{pmatrix}\rho_+(r)\\ \rho_-(r)\end{pmatrix},\end{aligned} \tag{2}$$

where $A_h = \begin{pmatrix}a & c\\ c & b\end{pmatrix}+$, $v_c(r) = l_B/r$, and $v_y(r) = e^{-\kappa r}/r$. Similarity transformation decouples the Yukawa term with eigenstates

$$\begin{aligned}\beta\mathcal{U}_{\rm tot} = &\frac{1}{2}\int dr dr' \rho_c(r) v_c(r-r')\rho_c(r')\\ &+ \frac{1}{2}\int dr dr' \rho_1(r) v_{y,1}(r-r')\rho_1(r')\\ &+ \frac{1}{2}\int dr dr' \rho_2(r) v_{y,2}(r-r')\rho_2(r'),\end{aligned} \tag{3}$$

where $v_{y,i}(r) = \lambda_i v_y(r)$ for $i = 1, 2$. The λ_i is

$$\begin{aligned}\lambda_1 &= a\cos^2\theta + 2c\sin\theta\cos\theta + b\sin^2\theta,\\ \lambda_2 &= a\sin^2\theta - 2c\sin\theta\cos\theta + b\cos^2\theta,\end{aligned}$$

and $\rho_i(r)$ is

$$\begin{aligned}\rho_1(r) &= \rho_+(r)\cos\theta + \rho_-(r)\sin\theta,\\ \rho_2(r) &= -\rho_+(r)\sin\theta + \rho_-(r)\cos\theta.\end{aligned}$$

Here, θ is

$$\tan 2\theta = \frac{2c}{a-b}. \tag{4}$$

The canonical partition function of the system is

$$\begin{aligned}\mathcal{Z}_c &= \sum_{\{n_\pm(r)\}} \delta\left(\sum_r n_+(r) - N_+\right)\delta\left(\sum_r n_-(r) - N_-\right) e^{-\mathcal{U}_{\rm tot}}\\ &= \sum_{\{n_\pm(r)\}} \delta\left(\sum_r n_+(r) - N_+\right)\delta\left(\sum_r n_-(r) - N_-\right)\\ &\quad\times \exp\left(-\frac{1}{2}\int dr dr' \rho_c(r) v_c(r-r')\rho_c(r')\right.\\ &\quad -\frac{1}{2}\int dr dr' \rho_1(r) v_{y,1}(r-r')\rho_1(r')\\ &\quad \left.-\frac{1}{2}\int dr dr' \rho_2(r) v_{y,2}(r-r')\rho_2(r')\right).\end{aligned} \tag{5}$$

It is more practical to deal with the grand canonical ensemble

$$\mathcal{Z}_\lambda = \sum_{N_+=0}^{\infty}\sum_{N_-=0}^{\infty} \frac{\lambda_+^{N_+}}{N_+!}\frac{\lambda_-^{N_-}}{N_-!}\mathcal{Z}_c,$$

where fugacities $\lambda_\pm$ are function of the chemical potential $\mu_\pm$, $\lambda_\pm = e^{\beta\mu_\pm}$. In equilibrium, satisfying charge neutrality conditions $\lambda_+ = \lambda_- = \lambda_s$.

The grand canonical partition function after the Hubbard-Stratonovich transformation yields

$$\begin{aligned}\mathcal{Z}_\lambda = &\int \mathcal{D}\phi_e \mathcal{D}\phi_1 \mathcal{D}\phi_2 \exp\left(-\frac{1}{8\pi l_B}\int dr(\nabla\phi_e)^2\right.\\ &-\frac{1}{8\pi\lambda_1}\int dr\left((\nabla\phi_1)^2 + \kappa^2\phi_1^2\right)\\ &\left.-\frac{1}{8\pi\lambda_2}\int dr\left((\nabla\phi_2)^2 + \kappa^2\phi_2^2\right)\right)\\ &\times\exp\left(\frac{1}{v}\int dr \ln\left(\lambda_s(\mathbf{e}_1 + \mathbf{e}_2)\right)\right),\end{aligned} \tag{6}$$

where $\mathbf{e}_1 = \exp(-i\phi_e - i\phi_1\cos\theta + i\phi_2\sin\theta)$ and $\mathbf{e}_2 = \exp(+i\phi_e - i\phi_1\sin\theta - i\phi_2\cos\theta)$. The free energy is

$$\begin{aligned}\beta\mathcal{F} = \int dr\Bigg[&-\frac{1}{8\pi l_B}(\nabla\psi_e)^2 - \frac{1}{8\pi\lambda_1}\left\{(\nabla\psi_1)^2 + \kappa^2\psi_1^2\right\}\\ &-\frac{1}{8\pi\lambda_2}\left\{(\nabla\psi_2)^2 + \kappa^2\psi_2^2\right\}\Bigg] + \eta(\tilde{\mathbf{e}}_1, \tilde{\mathbf{e}}_2),\end{aligned} \tag{7}$$

where

$$\eta(\tilde{\mathbf{e}}_1, \tilde{\mathbf{e}}_2) = -\frac{1}{\nu}\int dr \ln\{\lambda_s(\tilde{\mathbf{e}}_1 + \tilde{\mathbf{e}}_2)\},$$

and $\tilde{\mathbf{e}}_1 = \exp(-\psi_e - \psi_1\cos\theta + \psi_2\sin\theta)$ and $\tilde{\mathbf{e}}_2 = \exp(+\psi_e - \psi_1\sin\theta - \psi_2\cos\theta)$. We introduced θ to linearly separate the two Yukawa fields for the convenience of calculations. The saddle-point field approximates the functional integral as

$$\begin{aligned}
\frac{1}{4\pi l_B}\nabla^2\psi_e &= \frac{1}{\nu}\frac{\tilde{\mathbf{e}}_2 - \tilde{\mathbf{e}}_1}{\tilde{\mathbf{e}}_1 + \tilde{\mathbf{e}}_2},\\
\frac{1}{4\pi\lambda_1}(\nabla^2 - \kappa^2)\psi_1 &= \frac{1}{\nu}\frac{-\cos\theta\tilde{\mathbf{e}}_1 - \sin\theta\tilde{\mathbf{e}}_2}{\tilde{\mathbf{e}}_1 + \tilde{\mathbf{e}}_2},\\
\frac{1}{4\pi\lambda_2}(\nabla^2 - \kappa^2)\psi_2 &= \frac{1}{\nu}\frac{\sin\theta\tilde{\mathbf{e}}_1 - \cos\theta\tilde{\mathbf{e}}_2}{\tilde{\mathbf{e}}_1 + \tilde{\mathbf{e}}_2}.
\end{aligned} \tag{8}$$

While the point-charge model considers the source of the Coulomb interaction, our modified case deals with both sources of Coulomb and Yukawa interaction, similar to Ref. [27].

III. MOLECULAR DYNAMICS SIMULATION

We performed molecular dynamics (MD) simulations employing Ye's coarse-grained model, which successfully induced the divergence of differential capacitance [35]. To compare the simulation results with our theory, we modified the model by introducing asymmetric Yukawa interactions. All simulations were performed using LAMMPS [45] in the canonical ensemble and fundamental quantity scale input parameters and output quantities. The main dimensionless physical quantities are provided in Sec. A of the Supplemental Material [49].

In EDLCs simulations, it is crucial to treat the interactions between ions and electrodes properly. An image-charge method effectively accounts for the dielectric discontinuity between the electrolyte and the surrounding medium. When the relative permittivity of the bounding material is lower (higher) than that of the electrolyte, ions experience repulsion (attraction) with their images [43,44].

The image-charge method, implemented in LAMMPS by Dwelle and Willard [46], is based on the method proposed by Hautman *et al.* [47]. It involves considering infinitely repeating systems of image charges when simulating a three-dimensional system with ions. The simulation system is divided into two subsystems: a real system on the right side ($0 < x < L_x$) and an image system on the left side ($-L_x < x < 0$). The image particles possess charges opposite to those of the real particles in the real system, and they are generated at positions symmetric to the real particles relative to the electrode located at $x = 0$. The whole simulation box is repeated as a unit cell.

In this study, the system consists of 1000 real particles and 1000 image particles with a number density of $\rho = 0.8$, and the temperature is set to $T = 1$ using Langevin thermostat. The simulation box is created with the size of $2L \times L \times L$ where the value of L is determined to satisfy the desired number density $\rho = N/V$. Furthermore, wall potentials are applied at $x = 0$ and $x = L$ to represent two smooth planar electrodes. The relative permittivity ε_r and Bjerrum length l_B are set to typical values used for RTIL systems [19,39,48], i.e., $\varepsilon_r = 12$ and $l_B = 10$. Moreover, the elementary charges have reduced magnitudes of $q = \sqrt{\varepsilon_r l_B T} \simeq 11$.

In addition to the long-range Coulomb interaction, particles interact with each other through combined short-ranged pair potentials. The short-range ion-ion correlation is modeled by shifted Yukawa potential. For here, the potential has the form

$$\beta U_Y(r_{ij}^*) = \begin{cases} \dfrac{C_{ij}}{r_{ij}^*}(e^{-r_{ij}^*/l_c} - e^{-r_c^*/l_c}), & r_{ij}^* \leqslant r_c^* \\ 0, & r_{ij}^* > r_c^* \end{cases} \tag{9}$$

where C_{ij} represents Yukawa coefficient, which can be a for cation-cation, b for anion-anion, and c for cation-anion. Details of the rest of pair potentials are explained in Sec. B of Supplemental Material [49].

To investigate the effect of asymmetric Yukawa potential on the EDL formation, the zero-field simulations were performed. For convenience, correlation strengths between ions were expressed by scaling relative to the cation-cation correlation a., i.e., $b = a \times \alpha_b$, $c = a \times \alpha_c$. In simulations, a was fixed to -7.5 and α_b and α_c were varied within certain ranges: $0.1 \leqslant \alpha_b \leqslant 1.4$ and $0.9 \leqslant \alpha_c \leqslant 1.2$.

Subsequently, simulations with uniform electric field were performed to elucidate the effect of asymmetric Yukawa interaction on the formation of crowding structure. Electric fields with strength $-1 \leqslant E \leqslant 1$ were applied to model potential differences with strength $-118 \leqslant \Delta V/V_T \leqslant 118$. For here, $V_T = k_B T/e \approx 11$ is the thermal voltage in LJ units, and a and α_c were fixed to -7.5 and 1.1, respectively, while α_b is varied.

For all simulations, energy minimization and equilibration were performed over 10^5 time steps with a step size $\tau = 0.001$. Another $3 \times 10^6\tau$ steps were spent for data production.

In our efforts to align parameters between MD simulations and field-theoretic analysis, we encountered difficulties in observing the formation of EDLs when directly applying the theoretical parameters due to critical differences between the two methodologies. To observe and investigate the EDL structures such as overscreening and crowding, we adopted a parameter set of Ref. [35]. This does not provide direct comparisons but allows us to conduct qualitative comparisons between the theory and simulations by observing the response to the change of the Yukawa terms. The results of directly applying the theoretical parameters are provided in Sec. F of the Supplemental Material [49].

IV. THEORETICAL RESULTS

When the short-range interaction is symmetric, i.e., $a = b$, Eq. (8) yields

$$\begin{aligned}
\frac{\nu}{4\pi l_B}\nabla^2\psi_e &= \tanh(\psi_e + \psi_h),\\
\frac{\nu}{2\pi(c-a)}(\nabla^2 - \kappa^2)\psi_h &= \tanh(\psi_e + \psi_h),
\end{aligned} \tag{10}$$

where $\psi_h = -\psi_2/\sqrt{2}$. To check correspondences, we used boundary conditions [27,36]

$$\psi_e'(0) = -\kappa_e s_e,$$
$$\begin{pmatrix} \psi_1'(0) - \kappa\psi_1(0) \\ \psi_2'(0) - \kappa\psi_2(0) \end{pmatrix} = -4\pi A_h \begin{pmatrix} \sigma_1 \\ \sigma_2 \end{pmatrix}, \tag{11}$$

where $\kappa_e^2 = 4\pi l_B/\nu$ and $s_e = \kappa_e\sigma_e/e$. We set $\sigma_1 = \sigma_2 = 0$ for the simplicity. The numerical solutions of these nonlinear differential equations perfectly reproduce the previous results [27] (Fig. S2). Setting $a = b$ allows us to recover the equation in Ref. [27]. Further condition on c ($a = b = -c$) reduces our equation to BSK equation.

To capture the behavior of the more realistic systems, we study asymmetric cases $a \neq b$. We scale b and c relative to a, $b = a \times \alpha_b$, and $c = a \times \alpha_c$, respectively.

Under the condition of $\sigma_1 = \sigma_2 = 0$, we explore the influence of α_b by numerically solving Eq. (8), while fixing α_c. Figure 1(a) reveals a deviation of $s_e(\psi_0)$ from the symmetric solution, which transits at $\psi_0 = 0$. The emergence of hysteresis stems from the delayed reorganization of RTIL double layers during the increase of surface charge density. This also indicates a first-order phase transition, which can lead to charge separation [41,42]. The hysteresis in the $s_e(\psi_0)$ curve coincides with a divergence in the differential capacitance $\tilde{C}_{\text{diff}} = 1/(d\psi_0/ds_e)$, suggesting the first-order transition during EDL formation, consistent with the previous studies [27,36,41,42]. Notably, short-range attractions induce overscreening or crowding, which is rarely observed in pure electrostatic systems.

Next, we investigate the influence of the cation-anion interaction α_c. The surface charge density s_e is measured by varying α_b for a given α_c value, and repeated this process for multiple α_c values. Figure 1(b) demonstrates that increasing α_c shifts the onset of $\tilde{C}_{\text{diff}}$ divergence toward lower α_b. This intriguing trend can be attributed to the enhanced aggregation of like-charged ionic liquids at larger α_c. Stronger cation-anion attraction elevates the energy penalty associated with mixing oppositely charged species. We can get insight considering the effective interaction parameter $\xi = a(1 + \alpha_b - 2\alpha_c)$: as α_c increases, EDL transition becomes feasible even at lower α_b.

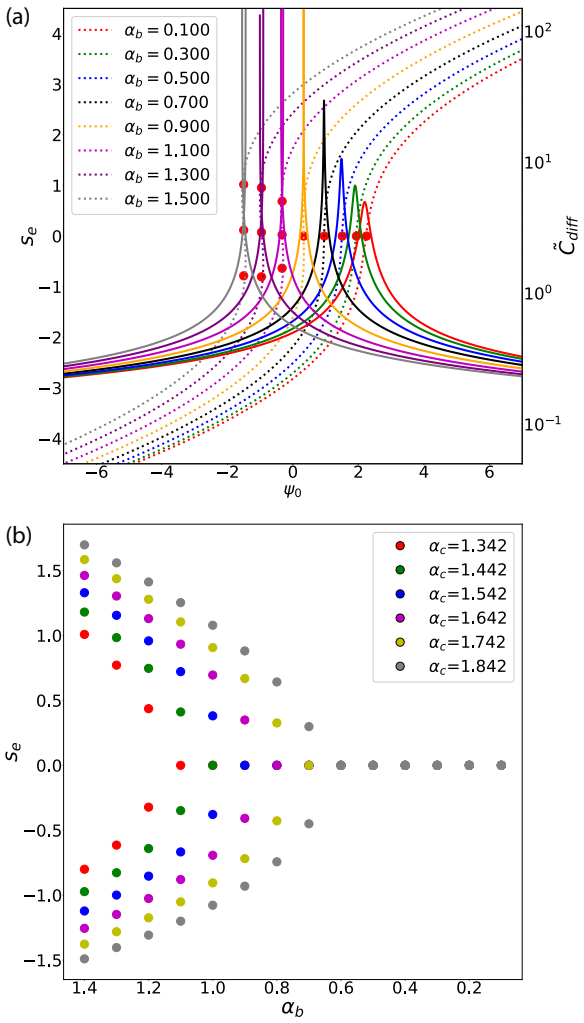

FIG. 1. (a) Scaled surface charge density (dotted) and scaled differential capacitance (solid) as a function of surface electrostatic potential by varying α_b values for fixed α_c. (b) Scaled surface charge density as a function of α_b for different values of α_c.; (a) α_b varies from 0.1 (most right) to 1.3 (most left) with an increment of 0.2 while fixing $\alpha_c = 1.442$. Red markers indicate ψ_0 at which $s_e = 0$. The discontinuous surface charge densities at $\alpha_b = 1.1$ says surface charge separation of the ions, and shows the onset divergence of the $\tilde{C}_{\text{diff}}$.

V. COMPARATIVE ANALYSIS OF MOLECULAR DYNAMICS SIMULATIONS AND THEORETICAL MODELS

The local charge-density profile $\rho_c(x) = q(\langle n_+(x)\rangle - \langle n_-(x)\rangle)$ is obtained by averaging simulation configurations, where $n_+(x)$ and $n_-(x)$ are the number densities of cations and anions, respectively. The densities are averaged over surface-parallel directions. The surface charge density is calculated by

$$s_e = \frac{\varepsilon_r \Delta V}{4\pi L_x} - \frac{1}{L_x}\int_0^{L_x} x\rho_c(x)dx, \tag{12}$$

where ΔV is the difference of constant potential between electrodes [35].

Zero-field simulations ($\Delta V = 0$) show the role of Yukawa potentials in forming EDLs without the charge-coupling effects. Figure 2(a) displays that spontaneous surface charge separation (SSCS) is absent until $\alpha_c = 0.9$. It emerges when α_c exceeds 1.0. In addition, the onset of SSCS shifts toward lower values of α_b as α_c increases. This is analogous to our theoretical results shown in Fig. 1(b). In other words, increasing α_c implies that charge separation occurs at lower α_b, indicating that charge separation occurs more easily, which qualitatively matches the theoretical results. Notably, despite exploring a reasonable range of Yukawa coefficients, the crowding in EDLs was absent in our zero-field simulations. The parameters inducing crowding structure without external field, in Ref. [35], lead to the void formation in our simulations, perhaps due to the unphysically strong Yukawa interactions.

Applying external potentials, the crowding appears across a wide range of the Yukawa coefficients. Figure 3 shows the crowding emerges above a certain external potential threshold,

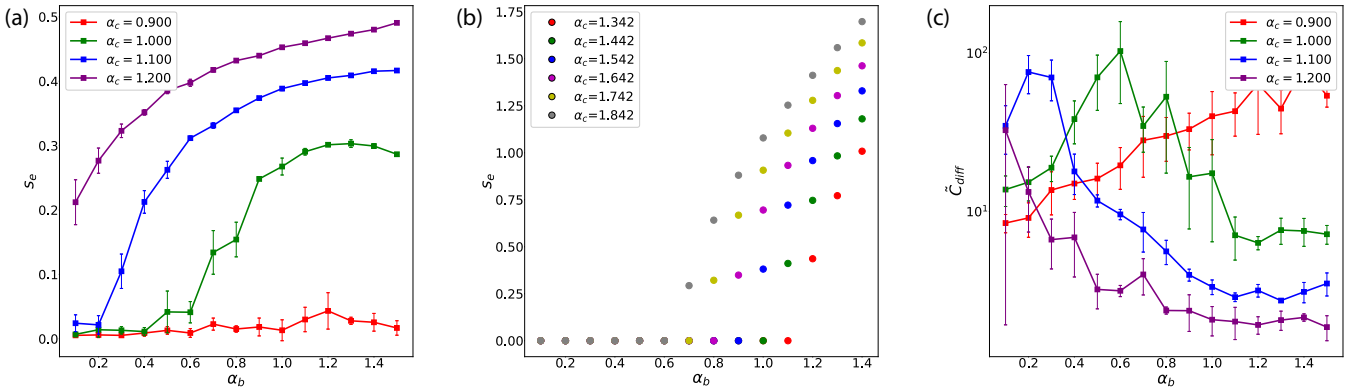

FIG. 2. MD results of charge separation and differential capacitance: (a) No spontaneous surface charge separation (SSCS) is observed below $\alpha_c = 0.9$. Above $\alpha_c = 1.0$, SSCS occurs, and the onset of SSCS shifts toward smaller α_b consistent with the theory. (b) The results of charge separation calculated from the field-theoretic results. Theory and simulation results are qualitatively similar in trends. (c) The peak of $\tilde{C}_{\text{diff}}$s emerge at the onset of SSCS. Without SSCS, $\tilde{C}_{\text{diff}}$ shows no peak.

while overscreening dominates below that value. Previous works [19,37] have identified the external field as a crucial factor governing the transition between overscreening and crowding. Interestingly, our model predicts overscreening, crowding, and bulk phase demixing despite low external fields. The short-range Yukawa interaction plays a critical role in spontaneous surface charge separation and multiple-layer formation inside EDL.

Without Yukawa interaction, the electric double layer is formed only when the coupling parameter ($\equiv 2\pi q^3 l_B^2 \sigma_e$ where q is valence of counterions) is very large. In reality, the condition can be achieved either when the surface charge density exceeds $1\text{e}/\text{nm}^2$ or counter ions are multivalent. However, ionic liquids exhibit EDL formation even at very low voltages, suggesting an additional driving force beyond simple charge coupling. The multipolar interactions and hardcore repulsion arising from the large, delocalized charges within the ionic liquid induce an alternative way of EDL formation.

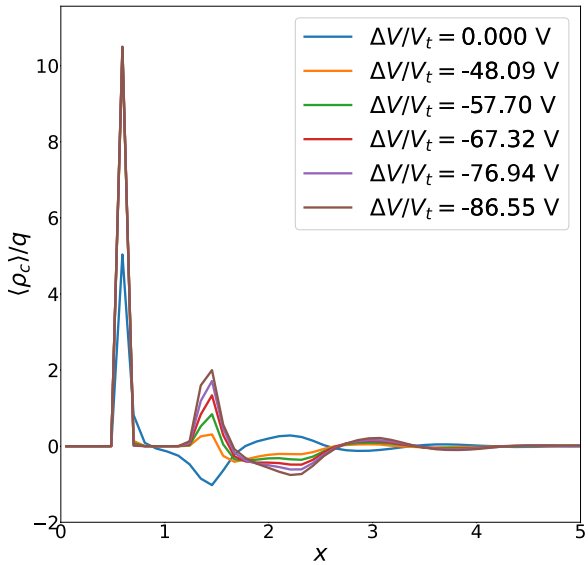

FIG. 3. Charge-density profiles obtained from the MD simulations by varying external field.

Our model captures these nonelectrostatic interactions through Yukawa interactions. In the limit that molecules carry zero charges, the effective short-range interaction may be described by $\chi = a(1 + \alpha_b - 2\alpha_c)$. But, in the opposite limit, for example, $\kappa = \infty$, ϕ_1 and ϕ_2 are zero, the coupling parameter $\Xi = q^2 l_B/\mu$ governs counterion condensation. In between, both parameters come into play, influencing the EDL formation. A negative value of χ leads to spontaneous surface charge separations. At the beginning of the simulation, two charges form local domains at both electrodes, which may be metastable due to large line tensions [35]. Given enough time, the metastable state transits to a stable state, in which a single charge species is abundant in each electrode [35,38]. The condensed layer easily overscreens the surface charges, which is extremely difficult to achieve for pure electrostatic cases.

In our case, because the Yukawa coefficients modify the electrostatic interactions also, χ cannot fully explain the surface phase demixing. For instance, increasing a or b has a distinct effect compared to decreasing c, even though both yield the same χ. This is because they also adjust the Coulombic interactions (in other words, the total interaction differs for both cases.). Smaller α_b makes large anionic domain formation difficult, while larger α_c enhances it. If α_c is unreasonably large enough to ignore the Coulomb interaction, it provokes a bulk phase transition of the binary demixing.

Within the parameter range explored in this study, an external field can induce the development of multiple layers of charges, also known as crowding, at the surface (see Fig. 3). While a large surface charge density is required to trigger crowding [39,40], the onset voltage varies depending on the Yukawa interactions. Stronger short-range repulsion between opposite charges or attraction between like charges reduces the onset voltage [Fig. 1(b)]. These findings highlight the interplay between the multipolar nature of the ionic liquid (which translates into the strength of the short-range interaction) and the external electric field in determining the overscreening and crowding inside EDL.

The internal structure of EDL at the divergence of $\tilde{C}_{\text{diff}}$ is controversial [19]. At the onset of divergence, our model reveals that the counterion arrangement is not determined by

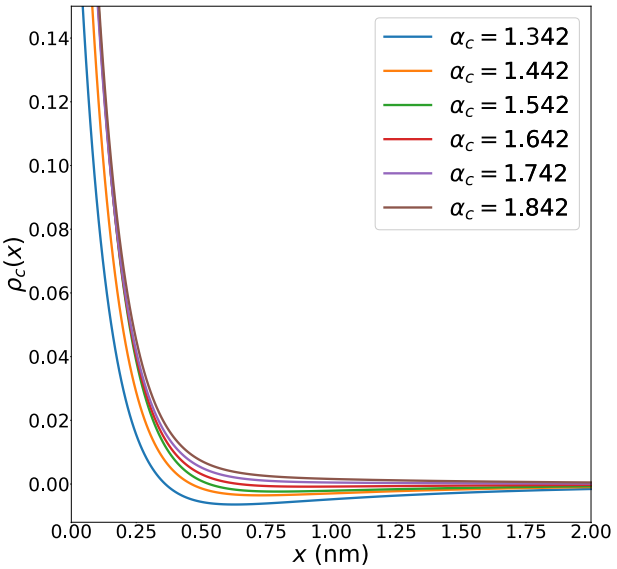

FIG. 4. Local charge-density profiles at the onsets of the $\tilde{C}_{\text{diff}}$ divergence obtained from the theoretical results.

a single EDL structure, such as conventional screening, overscreening, or crowding. To better understand, we investigate the local charge-density profiles at the onset of $\tilde{C}_{\text{diff}}$ divergence using our model. The average number of ions is

$$N_{\pm} = \lambda_{\pm} \frac{\partial \ln \mathcal{Z}_{\lambda}}{\partial \lambda_{\pm}}. \tag{13}$$

The local charge-density profile is obtained from the loop expansion adopted in the zeroth order:

$$\rho_c(r) = \sum_{i=\pm} \frac{N_i}{V} = \left\langle \frac{\tilde{e}_1 - \tilde{e}_2}{\tilde{e}_1 + \tilde{e}_2} \right\rangle = \frac{\bar{e}_1 - \bar{e}_2}{\bar{e}_1 + \bar{e}_2}, \tag{14}$$

where the potential in $\bar{e}_{1,2}$ is used as saddle-point solutions of ψ_e, ψ_1, and ψ_2. From the local charge-density profiles in Fig. 4, we find that condensed counterions screen the surface charge at $c \geqslant 1.742$. They start to overscreen the surface charge at $1.342 \leqslant c \leqslant 1.642$. It is plausible that large repulsion between different species may induce spontaneous surface charge separation even at low-surface charge densities and, hence, below the overscreening condition.

VI. LIMITING CASES

Some limiting behaviors may provide insights. Setting $a = b$ allows us to recover the equation in Ref. [27]. Further condition on $c\,(a = b = -c)$ reduces our equation to BSK equation. When $c \gg |a - b|$, $\theta \simeq \pi/4$, we can remove one of the fields to obtain a fourth-order differential equation since the Yukawa interaction is only meaningful between oppositely charged ILs. Conversely, if $c \ll |a - b|$, $\theta \simeq 0$, the Yukawa interactions are decoupled for each sign of charges so that one field is deduced by rewriting Eq. (8) in terms of $\psi_e + \psi_1$ and $\psi_e - \psi_2$.

If we assume that $\psi_e, \psi_1, \psi_2 \ll 1$, the differential equations in Eq. (8) can be linearized, and can be expressed only in terms of ψ_e. Linearization yields

$$\begin{aligned} \tilde{e}_1 &\simeq 1 - \psi_e - \psi_1 \cos\theta + \psi_2 \sin\theta, \\ \tilde{e}_2 &\simeq 1 + \psi_e - \psi_1 \sin\theta - \psi_2 \cos\theta. \end{aligned} \tag{15}$$

Using Eq. (15), we can re-express Eq. (8) as

$$\begin{aligned} \nabla^2 \psi_e &= \kappa_e^2 \psi_e + \frac{\kappa_e^2}{2} \psi_1 (\cos\theta - \sin\theta) \\ &\quad - \frac{\kappa_e^2}{2} \psi_2 (\cos\theta + \sin\theta), \\ \left(\nabla^2 - \kappa_1^2\right) \psi_1 &= -\alpha_1^2 \psi_e, \\ \left(\nabla^2 - \kappa_2^2\right) \psi_2 &= -\alpha_2^2 \psi_e, \end{aligned} \tag{16}$$

where $\kappa_e^2 = 4\pi l_B/\nu$, $\alpha_{1,2}^2 = -4\pi\lambda_{1,2}(\cos\theta - \sin\theta)/2\nu$, and $\kappa_{1,2}^2 = \kappa^2 + 4\pi\lambda_{1,2}/2\nu$.

When $\lambda_2 = 0$, the differential equation simplifies to a fourth-order equation. This condition is satisfied when $\tan\theta = 1$ or $\tan\theta = \frac{b}{a}$. The first condition corresponds to the symmetric case where $(a = b)$, while the second condition represents some asymmetric scenario where $2c = a + b$. In this case, the linearized equation of electrostatic potential becomes

$$\nabla^4 \psi_e - \left(\kappa_1^2 + \kappa_e^2\right) \nabla^2 \psi_e + \left(\kappa_1^2 \kappa_e^2 + \tilde{\alpha}_1^2\right) \psi_e = 0, \tag{17}$$

where $\tilde{\alpha}_1^2 = \alpha_1^2 \kappa_e^2 (\cos\theta - \sin\theta)/2$. Thus, small correction term $\tilde{\alpha}_1^2$ would be considered in the solution of ψ_e. We numerically solved the above equation and obtained $\psi_e(x)$ depending on the strength of Yukawa interaction. As shown in Fig. S7, when $a = b$, ψ_e shows exponential decay, indicating only real value of ω_1 and ω_2. However, if there is asymmetry between a and b, $\omega_{1,2}$ becomes a complex value, and this makes ψ_e oscillate.

Without assumption, in general, the linearized equation of electrostatic potential satisfies

$$\nabla^6 \psi_e - \xi \nabla^4 \psi_e + \mu \nabla^2 \psi_e - \chi \psi_e = 0, \tag{18}$$

where

$$\begin{aligned} \xi &= \left(\kappa_e^2 + \kappa_1^2 + \kappa_2^2\right), \\ \mu &= \left(\kappa_1^2 \kappa_2^2 + \kappa_e^2 \left(\kappa_1^2 + \kappa_2^2\right) + \tilde{\alpha}_1^2 + \tilde{\alpha}_2^2\right), \\ \chi &= \left(\kappa_e^2 \kappa_1^2 \kappa_2^2 + \tilde{\alpha}_1^2 \kappa_2^2 + \tilde{\alpha}_2^2 \kappa_1^2\right). \end{aligned}$$

Its solution of $\psi_e(x) = A_1 e^{-\omega_1 x} + A_2 e^{-\omega_2 x} + A_3 e^{-\omega_3 x}$, adopting boundary condition $\psi_e(x \to \infty) = 0$, we get

$$\begin{aligned} \omega_1^2 + \omega_2^2 + \omega_3^2 &= \xi, \\ \omega_1^2 \omega_2^2 + \omega_2^2 \omega_3^2 + \omega_1^2 \omega_3^2 &= \mu, \\ \omega_1^2 \omega_2^2 \omega_3^2 &= \chi. \end{aligned}$$

With the boundary conditions and linearized equations, we can find $\psi_0 = A_1 + A_2 + A_3$ by

$$\begin{aligned} \mathbf{MA} &= \mathbf{b}, \\ \mathbf{A} &= \mathbf{M}^{-1}\mathbf{b}, \end{aligned} \tag{19}$$

where

$$\mathbf{M} = \begin{pmatrix} \omega_1 & \omega_2 & \omega_3 \\ -\frac{\alpha_1^2(\omega_1+\kappa)}{\omega_1^2-\kappa_1^2} & -\frac{\alpha_1^2(\omega_2+\kappa)}{\omega_2^2-\kappa_1^2} & -\frac{\alpha_1^2(\omega_3+\kappa)}{\omega_3^2-\kappa_1^2} \\ -\frac{\alpha_2^2(\omega_1+\kappa)}{\omega_1^2-\kappa_2^2} & -\frac{\alpha_2^2(\omega_2+\kappa)}{\omega_2^2-\kappa_2^2} & -\frac{\alpha_2^2(\omega_3+\kappa)}{\omega_3^2-\kappa_2^2} \end{pmatrix},$$

$$\mathbf{A} = \begin{pmatrix} A_1 \\ A_2 \\ A_3 \end{pmatrix}, \qquad \mathbf{b} = \begin{pmatrix} \kappa_e s_e \\ s_1 \\ s_2 \end{pmatrix},$$

where $s_1 = -4\pi(a\sigma_1 + c\sigma_2)$ and $s_2 = -4\pi(c\sigma_1 + b\sigma_2)$. Thus, one can find analytic solution of ψ_0 by obtaining $\mathbf{M}^{-1}$. Differential capacitance also can be obtained by $\tilde{C}_{\text{diff}} = \frac{1}{\partial\psi_0/\partial s_e} = \sum_{i=1}^{3}(\partial A_i/\partial s_e)$.

VII. DISCUSSION

This study presents the intricate mechanisms of EDL formation at electrode-IL interface. It unveils the delicate interplay between two key interactions, the long-range Coulomb potential and the short-range Yukawa potential. The Yukawa potential arises from IL's large delocalized charges.

The Yukawa potential induces spontaneous surface charge separations (or charge condensation), and the Coulomb force enhances the condensation to develop further overscreening or crowding by reinforcing the strong coupling of counterions at the surface. At the onset of the divergence of differential capacitance, SSCS occurs. At this critical point, the external field may increase the condensed charges, but the coions would compensate them immediately.

No unique internal structure of EDLs arises at the onset of divergence of $\tilde{C}_{\text{diff}}$. The strength of short-range ion-ion correlations and surface charge density orchestrate the internal structure of EDLs. Considering these ionic liquids' properties, we can apply these results to real-world problems such as supercapacitors and solid-state electrolyte design.

ACKNOWLEDGMENTS

This research was supported by the National Research Foundation of Korea (NRF) grant funded by the Korea government (MSIT) Grants No. 2018M3D1A1058633 and No. 2021R1A2C1014562. This research was supported by Learning & Academic research institution for Master's ·Ph.D. students, and Postdocs (LAMP) Program of the National Research Foundation of Korea (NRF) grant funded by the Ministry of Education (Grant No. RS-2023-00301974).

[1] J. S. Wilkes and M. J. Zaworotko, Air and water stable 1-ethyl-3-methylimidazolium based ionic liquids, J. Chem. Soc. Chem. Commun. 965 (1992).
[2] R. D. Rogers and G. A. Voth, Ionic liquids, Acc. Chem. Res. **40**, 1077 (2007).
[3] C. Chiappe and D. Pieraccini, Ionic liquids: solvent properties and organic reactivity, J. Phys. Org. Chem. **18**, 275 (2005).
[4] M. Watanabe, M. L. Thomas, S. Zhang, K. Ueno, T. Yasuda, and K. Dokko, Application of ionic liquids to energy storage and conversion materials and devices, Chem. Rev. **117**, 7190 (2017).
[5] P. Simon and Y. Gogotsi, Perspectives for electrochemical capacitors and related devices, Nat. Mater. **19**, 1151 (2020).
[6] M. Armand, F. Endres, D. R. MacFarlane, H. Ohno, and B. Scrosati, Ionic-liquid materials for the electrochemical challenges of the future, Nat. Mater. **8**, 621 (2009).
[7] I. Osada, H. de Vries, B. Scrosati, and S. Passerini, Ionic-liquid-based polymer electrolytes for battery applications, Angew. Chem., Int. Ed. **55**, 500 (2016).
[8] E. Pomerantseva, F. Bonaccorso, X. Feng, Y. Cui, and Y. Gogotsi, Energy storage: The future enabled by nanomaterials, Science **366**, eaan8285 (2019).
[9] X. Chen, R. Paul, and L. Dai, Carbon-based supercapacitors for efficient energy storage, Natl. Sci. Rev. **4**, 453 (2017).
[10] L. Miao, Z. Song, D. Zhu, L. Li, L. Gan, and M. Liu, Ionic liquids for supercapacitive energy storage: A mini-review, Energy & Fuels **35**, 8443 (2021).
[11] P. R. Bueno, Nanoscale origins of super-capacitance phenomena, J. Power Sources **414**, 420 (2019).
[12] T. Sato, G. Masuda, and K. Takagi, Electrochemical properties of novel ionic liquids for electric double layer capacitor applications, Electrochim. Acta **49**, 3603 (2004).
[13] M. A. Gebbie, A. M. Smith, H. A. Dobbs, A. A. Lee, G. G. Warr, X. Banquy, M. Valtiner, M. W. Rutland, J. N. Israelachvili, S. Perkin, and R. Atkin, Long range electrostatic forces in ionic liquids, Chem. Commun. **53**, 1214 (2017).
[14] A. Eftekhari, Supercapacitors utilising ionic liquids, Energy Storage Materials **9**, 47 (2017).
[15] R. R. Netz and H. Orland, Beyond Poisson-Boltzmann: Fluctuation effects and correlation functions, Eur. Phys. J. E **1**, 203 (2000).
[16] L. Yan, Electrostatic correlations: from plasma to biology, Rep. Prog. Phys. **65**, 1577 (2002).
[17] C. D. Santangelo, Computing counterion densities at intermediate coupling, Phys. Rev. E **73**, 041512 (2006).
[18] A. Naji, M. Kanduč, J. Forsman, and R. Podgornik, Perspective: Coulomb fluids–weak coupling, strong coupling, in between and beyond, J. Chem. Phys. **139**, 150901 (2013).
[19] M. Z. Bazant, B. D. Storey, and A. A. Kornyshev, Double layer in ionic liquids: Overscreening versus crowding, Phys. Rev. Lett. **106**, 046102 (2011).
[20] V. Démery, D. S. Dean, T. C. Hammant, R. R. Horgan, and R. Podgornik, Overscreening in a 1D lattice Coulomb gas model of ionic liquids, Europhys. Lett. **97**, 28004 (2012).
[21] V. Démery, R. Monsarrat, D. S. Dean, and R. Podgornik, Phase diagram of a bulk 1D lattice Coulomb gas, Europhys. Lett. **113**, 18008 (2016).
[22] D. T. Limmer, Interfacial ordering and accompanying divergent capacitance at ionic liquid-metal interfaces, Phys. Rev. Lett. **115**, 256102 (2015).
[23] R. D. Coalson and A. Duncan, Systematic ionic screening theory of macroions, J. Chem. Phys. **97**, 5653 (1992).
[24] R. D. Coalson, A. M. Walsh, A. Duncan, and N. Ben-Tal, Statistical mechanics of a Coulomb gas with finite size

particles: A lattice field theory approach, J. Chem. Phys. **102**, 4584 (1995).
[25] R. R. Netz and H. Orland, Field theory for charged fluids and colloids, Europhys. Lett. **45**, 726 (1999).
[26] I. Borukhov, D. Andelman, and H. Orland, Adsorption of large ions from an electrolyte solution: a modified Poisson–Boltzmann equation, Electrochim. Acta **46**, 221 (2000).
[27] G. V. Bossa and S. May, Stability of ionic liquid modeled by composite Coulomb-Yukawa potentials, Phys. Rev. Res. **2**, 032040 (2020).
[28] J. P. De Souza and M. Z. Bazant, Continuum theory of electrostatic correlations at charged surfaces, J. Phys. Chem. C **124**, 11414 (2020).
[29] Y. A. Budkov, A. L. Kolesnikov, and M. G. Kiselev, A modified Poisson-Boltzmann theory: Effects of co-solvent polarizability, Europhys. Lett. **111**, 28002 (2015).
[30] R. R. Netz, Electrostatistics of counter-ions at and between planar charged walls: From Poisson-Boltzmann to the strong-coupling theory, Eur. Phys. J. E **5**, 557 (2001).
[31] A. Levy, D. Andelman, and H. Orland, Dipolar Poisson-Boltzmann approach to ionic solutions: a mean field and loop expansion analysis, J. Chem. Phys. **139**, 164909 (2013).
[32] P. Koehl, M. Delarue, and H. Orland, Simultaneous identification of multiple binding sites in proteins: A statistical mechanics approach, J. Phys. Chem. B **125**, 5052 (2021).
[33] S. J. de Carvalho, R. Metzler, and A. G. Cherstvy, Critical adsorption of polyelectrolytes onto charged janus nanospheres, Phys. Chem. Chem. Phys. **16**, 15539 (2014).
[34] D. L. Caetano, S. J. de Carvalho, R. Metzler, and A. G. Cherstvy, Critical adsorption of multiple polyelectrolytes onto a nanosphere: Splitting the adsorption–desorption transition boundary, J. R. Soc. Interface. **17**, 20200199 (2020).
[35] B. B. Ye and Z. G. Wang, A coarse-grained model of room-temperature ionic liquids between metal electrodes: a molecular dynamics study, Phys. Chem. Chem. Phys. **24**, 11573 (2022).
[36] Y. Avni, R. M. Adar, and D. Andelman, Charge oscillations in ionic liquids: A microscopic cluster model, Phys. Rev. E **101**, 010601 (2020).
[37] M. V. Fedorov and A. A. Kornyshev, Towards understanding the structure and capacitance of electrical double layer in ionic liquids, Electrochim. Acta **53**, 6835 (2008).
[38] R. Atkin, S. Z. El Abedin, R. Hayes, L. H. S. Gasparotto, N. Borisenko, and F. Endres, AFM and STM studies on the surface interaction of [BMP]TFSA and [EMIm]TFSA ionic liquids with Au(111), J. Phys. Chem. C **113**, 13266 (2009).
[39] A. A. Kornyshev, Double-layer in ionic liquids: Paradigm change? J. Phys. Chem. B **111**, 5545 (2007).
[40] X. Wang, M. Salari, D.-e. Jiang, J. Chapman Varela, B. Anasori, D. J. Wesolowski, S. Dai, M. W. Grinstaff, and Y. Gogotsi, Electrode materialionic liquid coupling for electrochemical energy storage, Nat. Rev. Mater. **5**, 787 (2020).
[41] H. Chao and Z.-G. Wang, Effects of surface transition and adsorption on Ionic liquid capacitors, J. Phys. Chem. Lett. **11**, 1767 (2020).
[42] M. Drüschler, B. Huber, S. Passerini, and B. Roling, Hysteresis effects in the potential-dependent double layer capacitance of room temperature ionic liquids at a polycrystalline platinum interface, J. Phys. Chem. C **114**, 3614 (2010).
[43] Y. S. Jho, M. Kanduč, A. Naji, R. Podgornik, M. W. Kim, and P. A. Pincus, Strong-coupling electrostatics in the presence of dielectric inhomogeneities, Phys. Rev. Lett. **101**, 188101 (2008).
[44] Y. S. Jho, M. W. Kim, P. A. Pincus, and F. L. H. Brown, A numerical study of the electrostatic properties of two finite-width charged dielectric slabs in water, J. Chem. Phys. **129**, 134511 (2008).
[45] S. Plimpton, Fast parallel algorithms for short-range molecular dynamics, J. Comput. Phys. **117**, 1 (1995).
[46] K. A. Dwelle and A. P. Willard, Constant potential, electrochemically active boundary conditions for electrochemical simulation, J. Phys. Chem. C **123**, 24095 (2019).
[47] J. Hautman, J. W. Halley, and Y. J. Rhee, Molecular dynamics simulation of water between two ideal classical metal walls, J. Chem. Phys. **91**, 467 (1989).
[48] C. Wakai, A. Oleinikova, M. Ott, and H. Weingärtner, How polar are ionic liquids? determination of the static dielectric constant of an imidazolium-based ionic liquid by microwave dielectric spectroscopy, J. Phys. Chem. B **109**, 17028 (2005).
[49] See Supplemental Material at http://link.aps.org/supplemental/10.1103/PhysRevResearch.6.033026 for detailed parameters and results from the MD simulations, schematic figures of conventional screening, overscreening, crowding, and the results of symmetric case, and linearized results of field theory.